Polarization-selective window-mirror effect in inductive gold grids

Benfeng Bai,[1,2,3,*] Janne Laukkanen,[1] Anni Lehmuskero,[1] Xiaowei Li,[2,3] and Jari Turunen[1]
[1]*Department of Physics and Mathematics, University of Eastern Finland, Joensuu Campus, P.O. Box 111, FI-80101 Joensuu, Finland*
[2]*State Key Laboratory of Precision Measurement Technology and Instruments, Department of Precision Instruments, Tsinghua University, Beijing 100084, China*
[3]*Tsinghua-Foxconn Nanotechnology Research Center, Tsinghua University, Beijing 100084, China*
(Received 11 May 2010; revised manuscript received 21 May 2010; published 16 June 2010)

A thin gold film perforated with an array of subwavelength holes is known to exhibit extraordinary transmission at normal incidence, irrespective of the state of polarization of illumination [T. W. Ebbesen *et al.*, Nature (London) **391**, 667 (1998)]. We report that, at slightly non-normal incidence (~8°), a properly designed inductive metal nanogrid may act as a window (with enhanced transmittance of 70%) or a mirror (with zero transmittance and enhanced reflectance) at a given wavelength, depending on the state of polarization of incident light. Experimental and numerical investigations reveal the role of surface plasmons as the underlying physical mechanism of this effect.

DOI: 10.1103/PhysRevB.81.235423 PACS number(s): 73.20.Mf, 42.79.Dj, 71.36.+c, 78.66.Bz

The extraordinary transmission effect mediated by surface plasmons in periodically perforated metal films has invoked much interest since its discovery[1] and has led to many important applications.[2] The debate on the physical mechanism of this effect (especially the positive or negative role of surface plasmons) is still ongoing,[3–6] but it is commonly agreed that the transmission effect involves two major contributions: the resonant excitation of propagating surface plasmon polaritons (SPPs) on the continuous metal surface and the direct scattering of light through the nanoholes.[7–10] The latter one is a nonresonant diffraction process, in which the localized fields within the volume of the holes are termed by different authors as cavity surface plasmons (CSPs),[7] propagating modes,[10] etc. Regardless of the difference of terminology, the field bounded to the metallic hole walls is in nature built up by collective oscillation of electrons[7] and is therefore also referred to as CSPs in this paper. The incident light can be coupled, via the diffraction Bloch modes of the grating, to both the SPPs and CSPs; it is the interference between the resonant and nonresonant processes that leads to the Fano-type profile of the transmission spectrum.[8,9]

Recently, Braun *et al.* reported on a suppressed transmission effect in a perforated ultrathin metal film where the strong coupling of SPPs on the upper and lower interfaces of the film is dominant.[11] It shows that perforated metal films may also produce suppressed transmission besides the well-known enhanced transmission effect.

In this paper, we report that a properly designed inductive metal nanogrid can exhibit a polarization-selective window-mirror effect at slightly non-normal incidence. That is, by altering the polarization direction of incident light, the inductive grid may act as a window (with enhanced transmission) or a mirror (with fully suppressed transmission and enhanced reflection) at a given wavelength. Different from Braun's structure,[11] the inductive grid studied in this work is thick enough to prevent the coupling of SPPs on the two interfaces; it is the interference of the lower-interface SPPs with the CSPs that leads to the window-mirror effect. We present experimental and theoretical explorations to reveal the underlying physics. The work may be helpful to the full understanding of the role of surface plasmons in the light transmission effect in perforated metal films and may lead to new applications such as light-switching plasmonic devices.

The investigated inductive grid, shown in Fig. 1(a), is a thin gold film perforated with an array of square holes on a fused silica substrate. The incident light lies in the *Oxz* plane containing one periodic direction and the grating normal, with the electric field vector perpendicular to (*s*-polarization) or in (*p*-polarization) the *Oxz* plane. The structure was designed to exhibit the polarization-selective transmission effect at a telecommunication wavelength $\lambda = 1300$ nm, by using the rigorous Fourier modal method for crossed gratings[12] for numerical optimization. The refractive index data of gold film used in simulation, which are considerably different from those of bulk gold, were measured by ellipsometry on a 100-nm-thick homemade gold film.[13]

We fabricated the inductive nanogrids by standard electron beam lithography and lift-off technique. Figure 1(b) shows a fabricated sample, whose parameters were measured as $d = 800$ nm, $h = 65$ nm, and $w = 375$ nm. Its transmittance and reflectance were characterized at various incident angles by spectroscopic ellipsometry (with a variable angle spectroscopic ellipsometer VASE produced by J. A. Woollam Co.) in the wavelength range 1000~1600 nm for the two polarization cases.

At normal incidence, the observed zero-order transmittance of the sample (not shown here) does not depend on the polarization direction of incident light, as expected, due to the symmetry of the configuration. However, when the angle of incidence deviates slightly from normal direction, the transmittance exhibits a sensitive dependence on polariza-

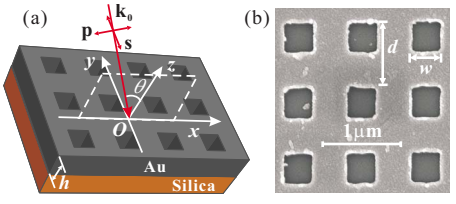

FIG. 1. (Color online) (a) Geometry of the inductive gold grid. (b) Scanning electron microscope image of a fabricated sample.

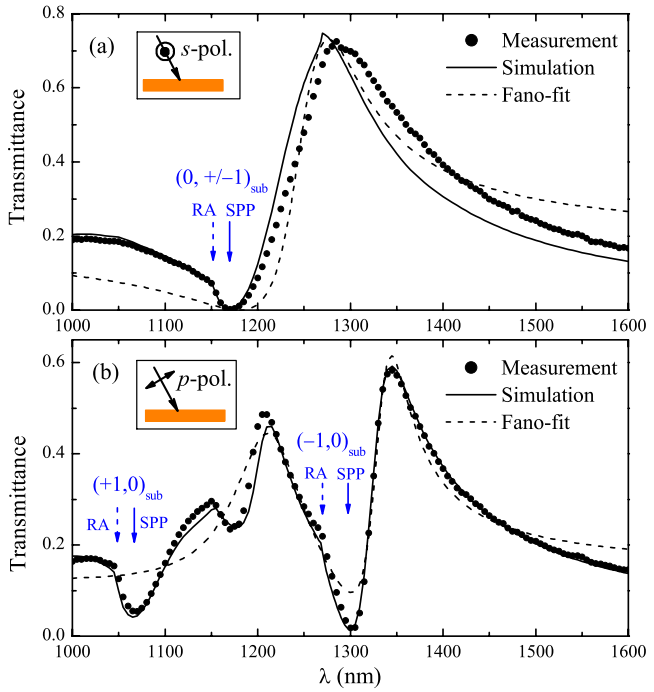

FIG. 2. (Color online) Measured (symbols), numerically calculated (solid lines), and Fano-profile fitted (dashed lines) zero-order transmittance of the sample under (a) *s*- and (b) *p*-polarized illuminations at incident angle $\theta=8°$. The dashed and solid vertical arrows indicate the positions of RAs and SPPs. The insets show the incident polarization configurations.

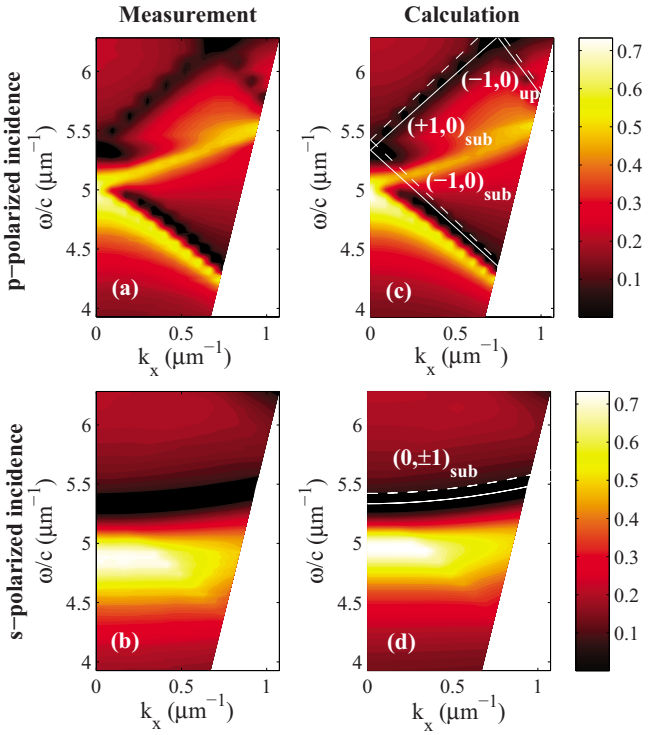

FIG. 3. (Color online) Measured and calculated zero-order transmittance of the inductive grid as a function of the in-plane wave-number k_x and angular frequency ω. The superimposed white solid and dashed lines are the dispersion curves of SPPs and RAs calculated with Eq. (1) and its revised form, respectively. "sub" and "up" indicate the substrate and upper interfaces.

tion. Figure 2 shows the measured transmittance spectra of the sample at an incident angle $\theta=8°$ under *s*- and *p*-polarized illuminations, which are in good agreement with the numerical simulations. For *s*-polarization, the transmittance curve is almost the same as in the normal incidence case, exhibiting an enhanced transmission peak of 70% around wavelength $\lambda=1300$ nm. Whereas, for *p*-polarization, a fully suppressed transmittance dip (nearly 0%) appears at the same wavelength. This indicates that, on the same sample at the same incident angle, we can switch between an extremely enhanced and suppressed transmission just by altering the polarization direction of incident light. For reference, a uniform gold film with the same thickness of 65 nm has a transmittance below 0.1%.

To understand the underlying physics, we first revisit the light-matter interaction process in metallic gratings. When light penetrates the metallic grid, it excites Bloch modes inside the grating layer, which are then coupled directly (a nonresonant process) or via SPPs (a resonant process) to radiative diffraction orders at the output surface of the grating.[14] In the inductive grid, the signature of nonresonant excitation of quasiperiodic Bloch modes can be observed as the periodically distributed CSPs localized on the walls of square holes (because the holes behave as effective electric dipoles under external electromagnetic excitation). Since this is a nonresonant process, the CSPs should be visible in a wide wavelength range, despite the variation of its field strength. The SPPs, however, can only be excited at certain wavelengths. The excitation condition of the (p,q)th-order SPP mode on a metallic grating surface is[6]

$$|\mathbf{k}_x + pK\hat{\mathbf{x}} + qK\hat{\mathbf{y}}| = k_0 \,\mathrm{Re}\sqrt{\epsilon_m\epsilon_d/(\epsilon_m+\epsilon_d)}, \qquad (1)$$

where $\mathbf{k}_x=k_0 \sin\theta\hat{\mathbf{x}}$ is the projection of incident wave-vector on the grating plane, $K=2\pi/d$, $\hat{\mathbf{x}}$ and $\hat{\mathbf{y}}$ are unit vectors in two periodic directions, $k_0=\omega/c$ is the vacuum wave-number, and ϵ_m and ϵ_d are the permittivities of metal and dielectric (air or silica), respectively. When the resonance condition of Eq. (1) is satisfied, one may observe a resonance feature (i.e., the rapid variation of intensity) in the diffraction spectra of the grating.

In addition, by replacing the right-hand-side of Eq. (1) with $\sqrt{\epsilon_d}k_0$, we can obtain the occurrence condition of Rayleigh anomaly (RA) (Ref. 15) corresponding to the cutoff of the (p,q)th diffraction order in the upper or lower space with permittivity ϵ_d.

Figure 3 demonstrates the measured and calculated transmittance spectra of the sample in the $k_x-\omega$ plane, where the dispersion curves of SPPs and RAs calculated with Eq. (1) and its revised form are superimposed. The positions of SPPs and RAs at $\theta=8°$ are also indicated in Fig. 2 on the transmittance spectra. It is seen that the dispersion curves of SPPs match perfectly with the traces of transmission dip, which is not fortuitous because the SPP mode of a flat metal film still survives on the residual metal surface of a perforated film as if it does not "see" the array of nanoholes.[4,7] The so-called modified SPP dispersion of a perforated metal film calculated with the S-matrix-pole method[4] is actually linked to the reso-

TABLE I. Fitting parameters of the Fano-profile transmittance of the inductive grid for *s*- and *p*-polarization cases.

	s-pol.	*p*-pol.(1)	*p*-pol.(2)
λ_{res} (nm)	1252	1212	1332
q	1.71	56.96	1.73
Γ (nm)	83.37	95.73	43.24
A	0.186	1.17×10^{-4}	0.142

nance of the whole geometry, involving the contribution of smooth-surface SPPs, CSPs, and other possible effects (such as the Fabry-Pérot resonance). The RAs are blueshifted a bit with respect to the SPP modes of the same order, which corresponds to the abrupt turning points on the transmittance spectra in Fig. 2.

Comparing the two polarization cases, we can see that the polarization-dependent transmission behavior arises from the lift of degeneracy of the SPP modes at oblique incidence. For *s*-polarization, in the spectral range of interest, only the $(0,\pm1)_{sub}$ SPP modes on the gold-silica interface are excited [consistently with the TM-excitation condition of SPPs (Ref. 6)], whose dispersion is still degenerate due to the symmetry of the two modes with respect to the incidence plane and exhibits small dependence on the incident angle θ. For *p*-polarization, however, the $(\pm1,0)_{sub}$ SPP modes are excited, whose dispersion is further split due to the asymmetrical excitation condition of the two modes in the incidence plane and is therefore very sensitive to θ. Consequently, as the transmittance of *s*-polarized case remains almost unchanged with respect to the normal incidence case with the increase of θ in the *Oxz* plane, the transmission peak of the *p*-polarized case turns drastically to a dip. By adjusting the splitting of SPP dispersion by incident angle θ, we can thereby achieve the polarization-switching enhanced and suppressed transmission at a given wavelength.

Now we proceed to analyze in depth the cause of the transmission peaks and dips. As stated before, the transmission behavior of a perforated metal film (whose resonance spectra usually have asymmetric profiles, as seen in Fig. 2) can be interpreted by Fano analysis[16] that accounts for the interference between a discrete process (in our case, the resonant excitation of SPPs) and a continuum (the nonresonant CSPs). With Fano's model,[16] the transmittance can be expressed as

$$T(\lambda) = A\frac{(q\Gamma/2+\lambda-\lambda_{res})^2}{(\lambda-\lambda_{res})^2+(\Gamma/2)^2}, \tag{2}$$

where q is an asymmetry factor defining the ratio of the resonant process over the nonresonant one, λ_{res} and Γ are the central wavelength and width of the resonance, and A is a free parameter normalizing the transmittance. Obviously, the *s*-polarized spectrum in Fig. 2 has one resonance and the *p*-polarized has two, due to the presence of different SPP modes. By fitting the spectra with Fano's model [for *p*-polarized case, Eq. (2) is extended as a sum of two terms depicting two resonances], we can draw the fitted curves (dashed lines in Fig. 2), with the fitting parameters listed in Table I, in which the last two columns correspond to the two resonances in *p*-polarized case. It is seen that the fitted curves can well reproduce the resonant features of the transmittance spectra, verifying that the transmission is indeed governed by the interference of a resonant and a nonresonant processes in the weak coupling regime[17] when the upper-surface SPPs of the metallic film do not couple with the lower-surface SPPs.

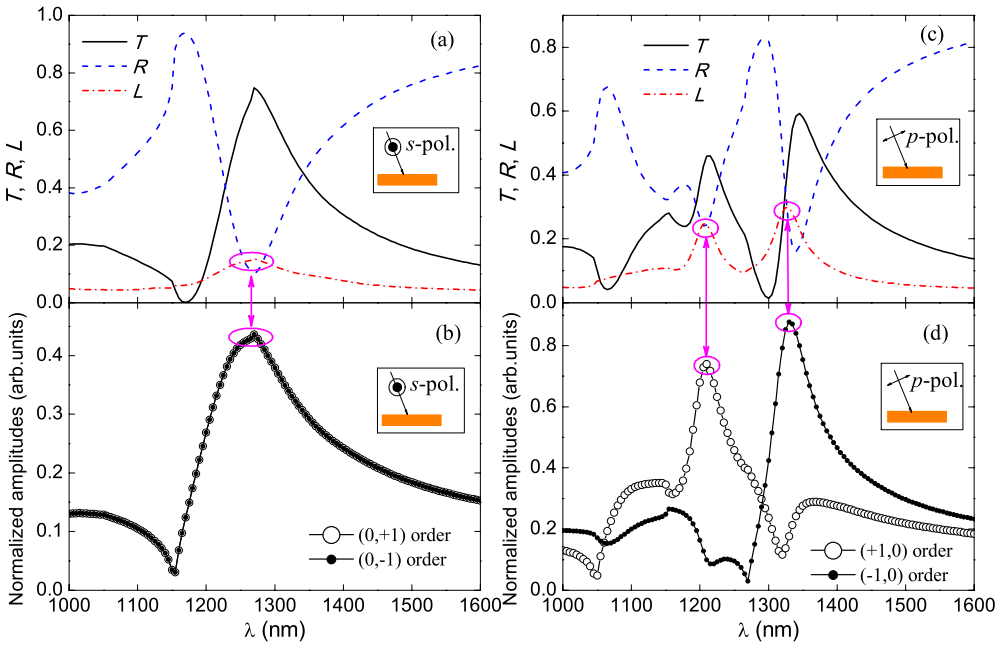

FIG. 4. (Color online) Numerically calculated zero-order transmittance T, reflectance R, total loss L, as well as the normalized amplitude modulus of the corresponding resonant diffraction orders for (a),(b) *s*- and (c),(d) *p*-polarization cases, in which the coincidence of the loss peaks with the amplitude peaks of diffraction orders is indicated by vertical arrows and ellipses.

However, it is noticed that the fitted central wavelengths of resonance (λ_{res} in Table I) coincide with neither the transmittance peak nor the dip, which appears difficult to understand at first sight. To reveal the underlying physics, we recall that the grating resonance is caused by energy transfer from the Bloch modes via the "resonant diffraction orders" (Ref. 15) to some guided or surface modes (in our case, the SPP modes). Therefore, the variation of strengths of the $(\pm 1,0)$ and $(0,\pm 1)$ transmitted orders that excite the corresponding SPP modes at the gold-silica interface must be examined.

In Fig. 4, we plot the numerically calculated zero-order transmittance T, reflectance R, total loss L, as well as the normalized amplitude modulus of the first transmitted orders. Two important facts are observed. First, the transmission peaks always correspond to the reflection dips and vice versa; while the loss peaks may be shifted away from the peak/dip positions of the transmittance and reflectance spectra (especially at the resonance around 1330 nm). Second, the amplitude peaks of the resonant diffraction orders are always in accordance with the loss peaks, just at the resonance wavelengths λ_{res} predicted by the Fano-fit. Specifically, in p-polarization case, the $(+1,0)$ and $(-1,0)$ orders contribute to the loss peaks around 1210 nm and 1330 nm, respectively; in s-polarization case, both the $(\pm 1,0)$ orders contribute to the loss peak around 1250–1270 nm.

The fitted q values in Table I imply that in this inductive grid the SPPs have strong interference with CSPs at each resonance except for the one at 1210 nm (for which $q \approx 57$), but the SPPs are dominant (for $q > 1$). As a result of the Fano interference, the transmission peak is redshifted from λ_{res} and a dip appears before λ_{res} simultaneously.

Based on the above analysis, we can conclude an intuitive physical picture of the light-matter interaction in the inductive grid. At resonance λ_{res}, the energy in Bloch modes couples strongly to SPPs and CSPs via the corresponding resonant diffraction order, which should cause a strong field confinement on the gold-silica interface and naturally raises the energy dissipation leading to the loss peak. At an offset wavelength smaller than λ_{res}, the resonance gets weaker while the excitation condition of SPPs on the residual smooth surface of the metal film is perfectly satisfied; the SPP-dominant field gives rise to a suppressed transmission and enhanced reflection. In contrast, at a wavelength longer than λ_{res}, CSPs should take a dominant role, compared with the weaker SPPs, which facilitates the enhanced transmission and suppresses the reflection. This conclusion is consistent with that of a recent study conducted with another analytical model.[7]

To corroborate the above explanation, we have numerically calculated the field distribution and energy flow (the time-averaged Poynting vector) on the upper and lower interfaces of the inductive grid. Figure 5 shows the distribution of electric field components $E_{\parallel} \equiv (E_x^2 + E_y^2)^{1/2}$ and E_z above the two interfaces for p-polarized case at $\lambda = 1330$ nm (a loss peak position). We can intuitively see the stronger field confinement on the lower interface [due to the excitation of the $(-1,0)_{sub}$ SPP mode] and a signature of the interference of the SPP mode (indicated by the left-propagating energy flow and the widely distributed E_z component on the residual smooth metal surface) with the CSPs (indicated by the dipolelike localized $E_{\parallel}$ component within the holes).

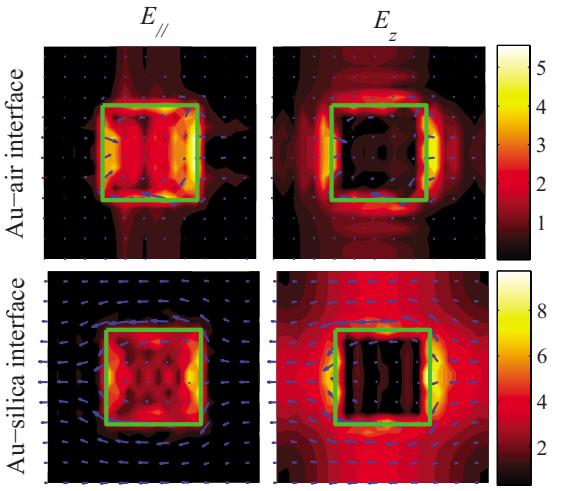

FIG. 5. (Color online) Distribution of the amplitudes of $E_{\parallel}$ and E_z (color plot, in the unit of incident field amplitude) and the energy flow (arrows with the arrow length proportional to the magnitude of the time-averaged Poynting vector) on the upper and lower interfaces for p-polarized case at $\lambda = 1330$ nm.

At other wavelengths, we can calculate the near-field distribution likewise. Since in the spectral range of interest the lower-interface SPPs are dominant (as seen from Figs. 2 and 3), we show in Fig. 6 only the E_z distribution and energy flow on the lower interface at six typical wavelengths. It is seen that, in p-polarization case, when λ deviates from the resonance wavelength 1330 nm, the near field becomes weaker (leading to less energy dissipation) and exhibits a pure SPP-like feature at 1300 nm (corresponding to a transmission dip) and an evident electric-dipole-like CSP feature at 1345 nm (corresponding to a transmission peak), indicating the dominant SPP mode and CSPs, respectively. At 1065 nm (the other transmission dip), the right-propagating energy flow indicates the presence of the $(+1,0)_{sub}$ SPP mode. In s-polarization case, the fields at the transmittance peak (1270 and 1300 nm) and dip (1170 nm) also exhibit the dominant CSP feature and SPP feature [the standing wave pattern

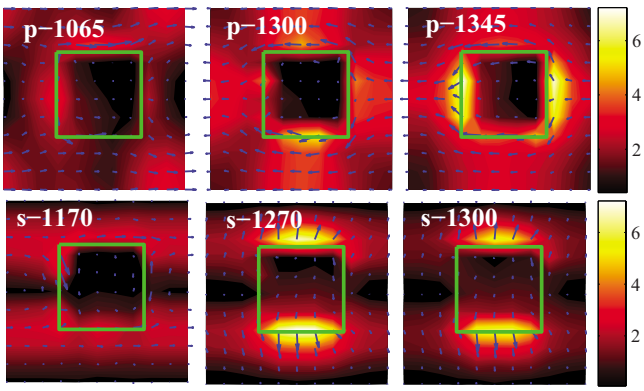

FIG. 6. (Color online) The same as Fig. 5 but for E_z and energy flow on the gold-substrate interface for six cases. The labeled white text in each plot reads "polarization-wavelength (nm)."

caused by the interference of the $(0,\pm 1)_{sub}$ SPP modes], respectively. These intuitive near-field calculations coincide with the explained physical process very well.

In conclusion, we have reported a polarization-switching enhanced/suppressed transmission effect in an inductive metal nanogrid operating at a telecommunication wavelength of 1300 nm under small incident angle. By exploring the underlying mechanism, we revealed the contributions of SPPs and CSPs in this effect. The study is helpful to the full understanding of the role of surface plasmons in the light transmission effect in perforated metal films and may lead to new applications such as light-switching plasmonic devices.

We acknowledge the support by the Academy of Finland (Projects No. 128420, No. 209806, and No. 129155), the Finnish Graduate School of Modern Optics and Photonics, and the National Basic Research Program of China (Project No. 2007CB935303).

*Corresponding author; baibenfeng@tsinghua.edu.cn

[1] T. W. Ebbesen, H. J. Lezec, H. F. Ghaemi, T. Thio, and P. A. Wolff, Nature (London) **391**, 667 (1998).
[2] S. A. Maier, *Plasmonics: Fundamentals and Applications* (Springer, New York, 2007).
[3] Q. Cao and P. Lalanne, Phys. Rev. Lett. **88**, 057403 (2002).
[4] P. Lalanne, J. C. Rodier, and J. P. Hugonin, J. Opt. A, Pure Appl. Opt. **7**, 422 (2005).
[5] W. L. Barnes, W. A. Murray, J. Dintinger, E. Devaux, and T. W. Ebbesen, Phys. Rev. Lett. **92**, 107401 (2004).
[6] A. V. Zayats and I. I. Smolyaninov, J. Opt. A, Pure Appl. Opt. **5**, S16 (2003).
[7] C. P. Huang, Q. J. Wang, and Y. Y. Zhu, Phys. Rev. B **75**, 245421 (2007).
[8] C. Genet, M. P. van Exter, and J. P. Woerdman, Opt. Commun. **225**, 331 (2003).
[9] M. Sarrazin, J.-P. Vigneron, and J.-M. Vigoureux, Phys. Rev. B **67**, 085415 (2003).
[10] P. B. Catrysse and S. Fan, Phys. Rev. B **75**, 075422 (2007).
[11] J. Braun, B. Gompf, G. Kobiela, and M. Dressel, Phys. Rev. Lett. **103**, 203901 (2009).
[12] L. Li, J. Opt. Soc. Am. A **14**, 2758 (1997).
[13] A. Lehmuskero, M. Kuittinen, and P. Vahimaa, Opt. Express **15**, 10744 (2007).
[14] E. G. Loewen and E. Popov, *Diffraction Gratings and Applications* (Marcel Dekker, New York, 1997).
[15] A. Hessel and A. A. Oliner, Appl. Opt. **4**, 1275 (1965).
[16] U. Fano, Phys. Rev. **124**, 1866 (1961).
[17] D. Gérard, L. Salomon, F. de Fornel, and A. Zayats, Opt. Express **12**, 3652 (2004).